International Journal of Microwave and Wireless Technologies

cambridge.org/mrf

Design and analysis of circular microstrip patch probe array for precise specific absorption rate measurement at quad-band

Bhukya Venkanna Naik[1,2]

[1]CSIR-National Physical Laboratory, Dr. KS Krishnan Marg, New Delhi-110012, India and [2]Academy of Innovative and Scientific Research (AcSIR), Ghaziabad-201002, India

Research Paper

Cite this article: Naik BV (2023). Design and analysis of circular microstrip patch probe array for precise specific absorption rate measurement at quad-band. *International Journal of Microwave and Wireless Technologies* **15**, 120–128. https://doi.org/10.1017/S1759078722000101

Received: 22 July 2021
Revised: 10 January 2022
Accepted: 11 January 2022
First published online: 7 February 2022

Keywords:
Specific absorption rate; microstrip patch; antenna array; mannequin; rectangular slot

Author for correspondence:
Bhukya Venkanna Naik,
E-mail: bvnaik@ieee.org

Abstract

This paper distinguishes the design and analysis of 3 × 2 circular microstrip patch probe array for specific absorption rate (SAR) measurement at quad-band. This novel approach consists of FR4 substrate radial dimension of 88 mm and it has six circular array elements with a radius of 17 mm; out of these six elements, three array elements are having rectangular slots with dimensions of $1.8 \times 1.5 \times 1.5\ mm^3$. The array elements are coupled with six probes which have a dimension of 100 mm with a 2.5 mm tip radius; these six probes are embedded into a tissue-equivalent liquid-filled human head mannequin. In this mannequin, instantaneous SAR at any six positions has been investigated. The proposed design resonates at 1.8, 2.1, 2.4, and 2.5 GHz with a return loss of −11.53, −15.90, −15.73, and −25.49 dB. The circular microstrip probe array is fed by a 50 Ohm coaxial feed. In addition, the 3D human head model analysis is also presented. The precisely estimated SAR values are 0.135, 0.108, 0.167, and 0.244 W/kg at 1 g of tissue. For the traceable measurements, each source of uncertainty budget has been estimated.

Introduction

The possible risk to human health from the electromagnetic energy emitted by everyday communication devices such as mobile phones, base station towers, Wi-Fi devices [1], etc. For several decades, researchers have tried to investigate the analysis of human head specific absorption rate (SAR) [2–6], but because of human tissue complexity, the precise SAR evaluation has not been done so far. And also, previous studies have been reported regarding electromagnetic waves on the human head in [7–9]. According to IEEE 1528, the electromagnetic energy measured in SAR, therefore, the specific absorption rate (SAR) is the rate at which how much energy is absorbed by biological tissue when exposed to RF sources, with the following equation (1).

$$\mathrm{SAR} = \frac{\sigma E^2}{\rho} \quad W/\mathrm{kg}, \tag{1}$$

whereas σ is the tissue conductivity (S/m), E is the electric field (V/m), and ρ is the mass density of the tissue for a human head ($1000\ kg/m^3$).

In the present existing wireless communication world, antennas are needed for daily usage communication, to assure the safety of the biological body from electromagnetic radiation. For that some of the guiding and protecting organizations, i.e. Federal Communication Commission (FCC), the European International Electrotechnical Commission (IEC62209-3) and IEEE 1528, International Commission on Non-ionization radiation protection (ICNIRP), have set a safety limit of 1.6 W/kg absorbed by 1 g tissue and 2 W/kg for 10 g tissue [1, 10, 11]. The important parameters in this problem are human tissue-equivalent complex permittivity, i.e.

$$\varepsilon^* = \varepsilon' - j\varepsilon'', \tag{2}$$

where ε' corresponds the real part energy store, remit energy and ε'' is imaginary part energy absorption. The both ratio called loss factor, in generally expressed in terms of loss tangent as given in equation (3)

$$\tan\delta = \frac{\varepsilon''}{\varepsilon'}. \tag{3}$$

In the biomedical application measurement tissue, conductivity and permittivity play a wider role with a respective frequency band that is in terms of the imaginary part of tissue, i.e.

$$\sigma = \omega\varepsilon''\varepsilon \quad \mathrm{S/m}, \tag{4}$$

where $\omega = 2\pi f$ is the measurement frequency and ε is the permittivity of free space.

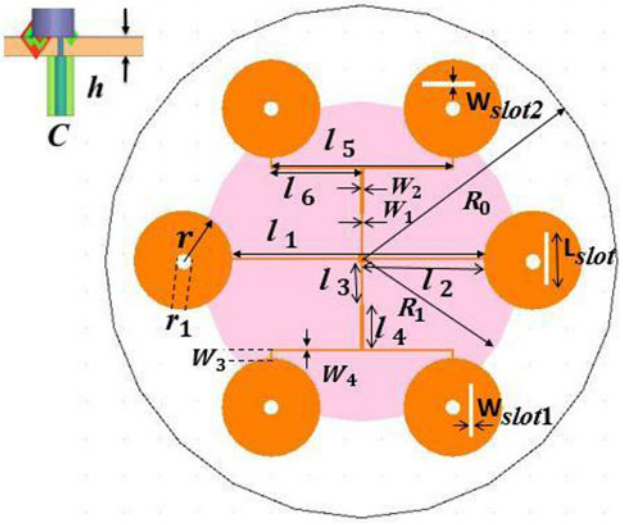

Fig. 1. The geometry of the proposed array.

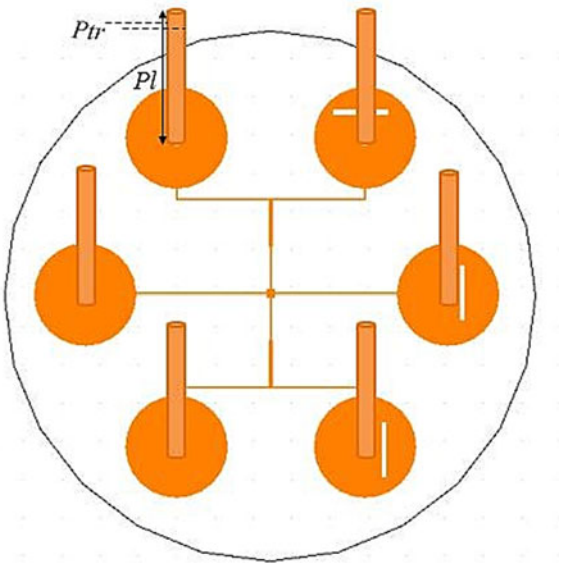

Fig. 2. The geometry of the proposed array with incorporated probes.

The previous studies have been explained regarding human head models as follows, Gandhi *et al*. reported the child's head and adult head comparison, Bernardi and Pisa claimed that SAR and temperature increase in the head of cellular-phone user [12], and Swadi and Abduljabar presented modelling of mobile electromagnetics wave effects on the human head [13]. Jamal *et al*. also presented an interaction of electromagnetic fields (100 kHz–30 GHz) exposure concerning human body model and methods for SAR measurement [14] and the vector probe array have been reported in IEC62209-3.

As per the literature survey concern up to date, none of the researchers reported regarding this concept. This study presents the evaluation of instantaneous electric field, i.e. SAR, at any six positions on the human head mannequin. The tissue conductivity, real and imaginary values are measured with the help of DAK probe [15]. Hence, the SAR values have been measured according to equation (1). Moreover, with the help of a robotic arm, precise measurements have been investigated. An advantage of the study is simultaneous E-field evaluation at six positions in the head of mannequin model. It measures precise SAR measurements that have been investigated in the human head phantom as well as the human body. This study may help monitor and maintain the international standards of SAR. The precise SAR evaluations have been needed in biomedical application and medical diagnostics; the design and analysis of the array are as follows.

Design and analysis

In this study, the novelty is the circular microstrip probe array that works at quad-band frequencies and measures the instantaneous electric field at six different positions in the human mannequin model; therefore, the precise SAR has been evaluated as per equation (1), and the circular microstrip probe array geometrical structure are shown in Figs 1 and 2.

The geometry consists of FR-4 epoxy substrate with an epsilon value of 4.4 and a loss tangent of 0.02, the thickness of the substrate h is 1.6 mm, overall radius of the substrate is R_o from the center and each circular element radius of r. Each circular element has incorporated probes, which has length P_l with a tip diameter of Pt_r; out of these six circular elements, three circular elements incorporated rectangular slots with dimensions of $W_{slot1,2}$ mm^3. These three slotted elements are on the right side of the circular microstrip as shown in Fig. 1, and the detailed dimensions are given in Table 1. The proposed circular array probe design is fed by a 50 ohm coaxial probe feed with a 3.5 mm connector, and with a 50 ohm input fed line width of W_1 and a 100 ohm output fed line width of W_2, as shown in Table 1. The design equations for the circular patch probe array antenna are as

Table 1. Dimensions of the circular microstrip patch probe array

Parameters	Dimensions in (mm)
Substrate material	FR4
Substrate thickness (h)	1.6
Dielectric constant (ε_r)	4.4
The radius of substrate (R_0)	88
Ground sunstrate radius (R_1)	55
Loss tangent (tanδ)	0.02
Slot width ($W_{slot1,2}$)	1.8, 1.5
Slot length (L_{slot})	18
Probe length(P_l)	100
Probe tip diameter (Pt_r)	2.5
Coaxial feed (C)	1.6
R	17
r_1, l_1	2.5, 86.33
l_2, l_3	43.31, 13.77
l_4, l_5	15.11, 63.22
l_6	30.80
W_1, W_2	0.7, 1.6
W_3, W_4	3, 0.7

https://doi.org/10.1017/S1759078722000101 Published online by Cambridge University Press

follows, from equation (5) to (8) [16, 17].

$$R_o = \frac{F}{\left\{1 + \frac{2h}{\pi\varepsilon_r F}\left[\ln\left(\frac{\pi F}{2h}\right) + 1.7726\right]\right\}^{0.5}}, \quad (5)$$

$$F = \frac{8.791}{f_r\sqrt{\varepsilon_r}}, \quad (6)$$

$$f_r = \frac{1.84 * c}{2\pi R_o\sqrt{\varepsilon_r}}, \quad (7)$$

where h is substrate thickness, f_r is resonance frequency in GHz, c is the velocity of the light, ε_r is dielectric permittivity.

For 50 ohms, coaxial feed line impedance matching estimation was performed as per the given below equation.

$$Z_0 = \sqrt{z_{in} \times z_l}. \quad (8)$$

Topological optimization

In the topological structural process, the parametric analysis is one of the important optimization techniques to achieve the desired results with respective proposed microstrip antenna geometry. In this section, we investigated the effect of rectangular slot width and length variation on the circular elements. When there was no additional slot present on the circular patch, the array shows a non-resonance behavior at the desired frequency, and hence, the analysis was arranged in such a way that, the slot width $W_{slot} = 0.5$–1.5 mm and slot length $L_{slot} = 1$–18 mm. From this observation, resonance varies with respective to return loss, and it has been presented in Figs 3(a) and 3(b). While incorporating the additional slots on the circular patch to enhance the impedance matching of the antenna, the patch resonates at 1.8–3 GHz, and therefore brings the response at desired frequencies of 1.8, 2.1, 2.1, and 2.5 GHz. Further, two more slots are incorporated on the circular patch. Finally, three slots are incorporated on the circular patch then the circular microstrip patch probe array resonated at desired quad-band frequencies; the obtained results are as shown in Figs 3 and 4.

Figures 3(a) and 3(b) show the impact of slot width on resonant frequency and impedance matching conditions at the circular patch are greater than its length. The resonance frequency is directly proportional to slot width, while impedance remains nearly constant. The detailed descriptions are as follows.

Figure 3a shows the variation of slot width with resonance frequency but slot length should be kept constant at 18 mm. With increasing value of slot width from 0.5 to 1.5 mm, the resonance frequency shifts toward the lower side at 1.5 mm. The acquired desired resonance frequencies are of 1.8, 2.1, 2.45, 2.5 GHz.

Figure 3b demonstrates the circular array element slot length varies from 1 to 18 mm with respective resonance frequency and the slot width kept constant at 1.5 mm; meanwhile, slot length varies from 1 to 18 mm. When the slot length is 1–17 mm, the observed resonance range is of 17–2.45 GHz, and hence, whenever increasing to a further value of 18 mm, the resonance response and enhanced impedance matching have been

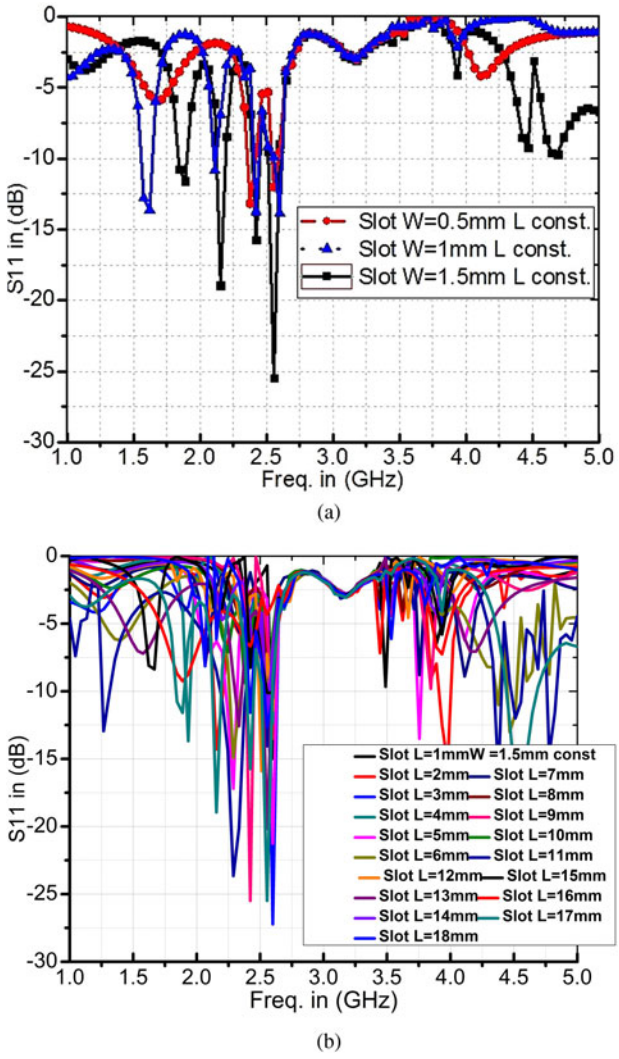

Fig. 3. (a) Slot width varies with a constant slot length, (b) slot length varies with a constant slot width.

observed at desired frequencies, therefore, the obtained accurate results are shown in Fig. 4.

Figures 5–9 present the E-field, current distribution, gain, efficiency, and the radiation pattern of the probe array at 1.8–2.5 GHz, as per the theory of fundamental transverse magnetic (TM_{10}) mode in microstrip patch antennas [16, 17], the E-field is maximum where current is minimum at the center of any patch, both *vice versa*. In the case of the proposed circular patch probe array, the E-field is maximum toward the probe and the surface current is maximum at the center of the circular patch. The total gain of the array is around 4.3 dB, the efficiency of the array is 80–90% at 1.8–2.5 GHz as shown in Fig. 8, and the circular probe array radiation patterns are omnidirectional and radiation is high at 1.8–2.5 GHz as shown in Fig. 9.

Analytical analysis of electromagnetic wave interaction to human head tissue

When electromagnetic energy interacts with the human head or biological body, it may cause harm to health because of mobile phones and other regularly used RF and microwave

https://doi.org/10.1017/S1759078722000101 Published online by Cambridge University Press

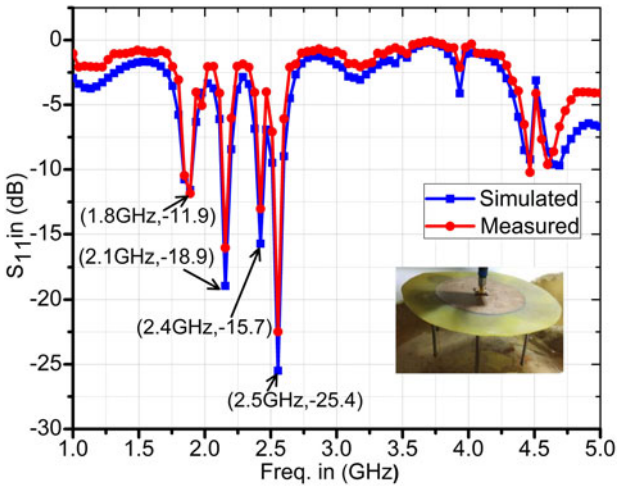

Fig. 4. The return loss of proposed antenna at 1.8–2.5 GHz.

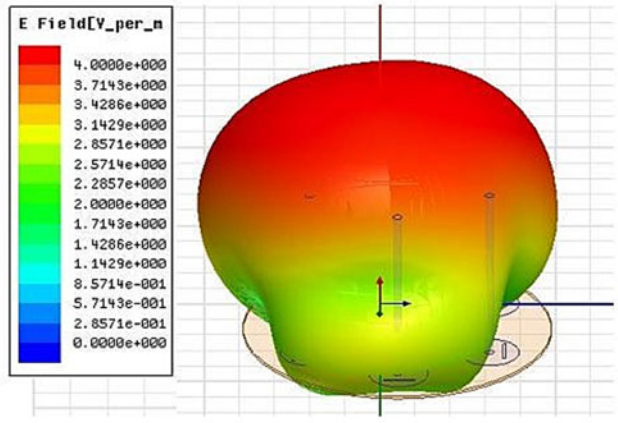

Fig. 5. Simulated E-field distribution.

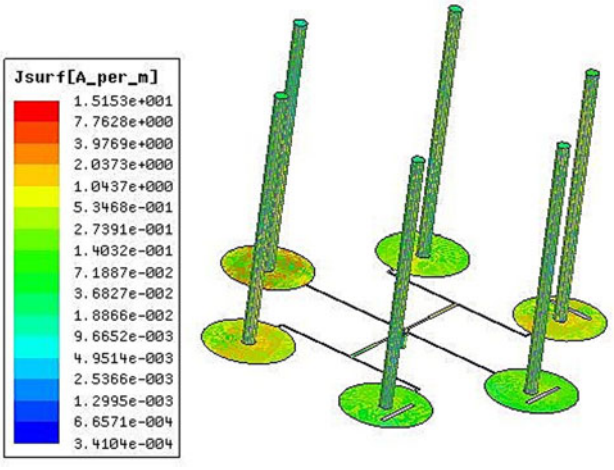

Fig. 6. Surface current distribution.

communication devices. In the analytical analysis environment, some assumptions are made to predict the electric field and temperature distribution on the human head as shown in equation (15).

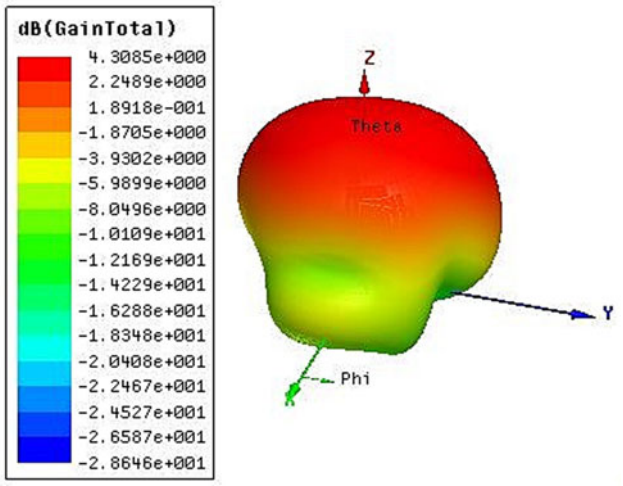

Fig. 7. Gain (3D view) of the array.

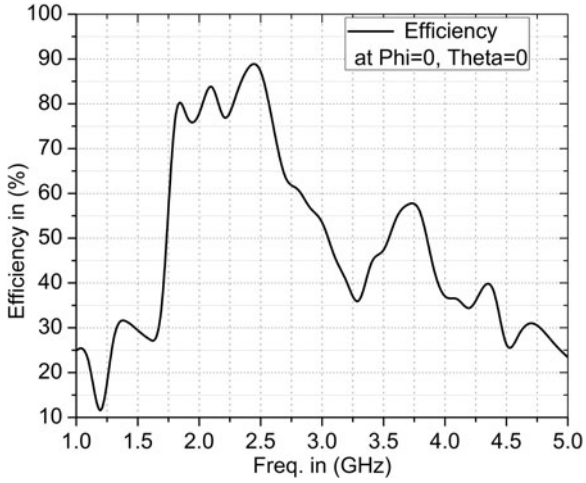

Fig. 8. The efficiency of the array.

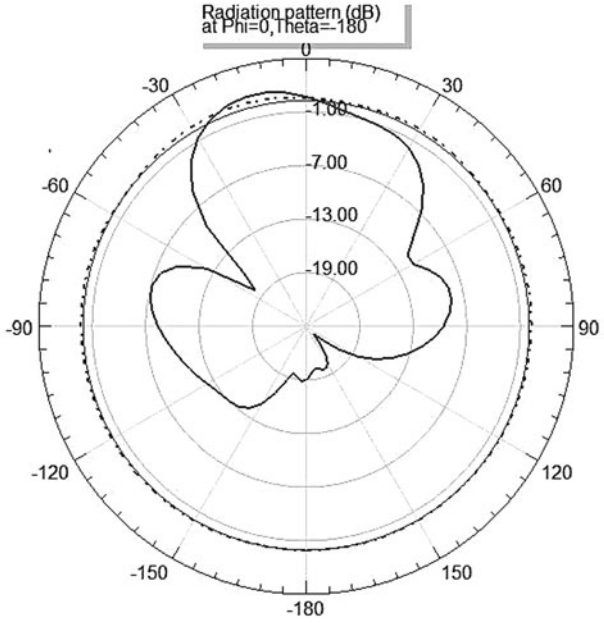

Fig. 9. Radiation pattern.

https://doi.org/10.1017/S1759078722000101 Published online by Cambridge University Press

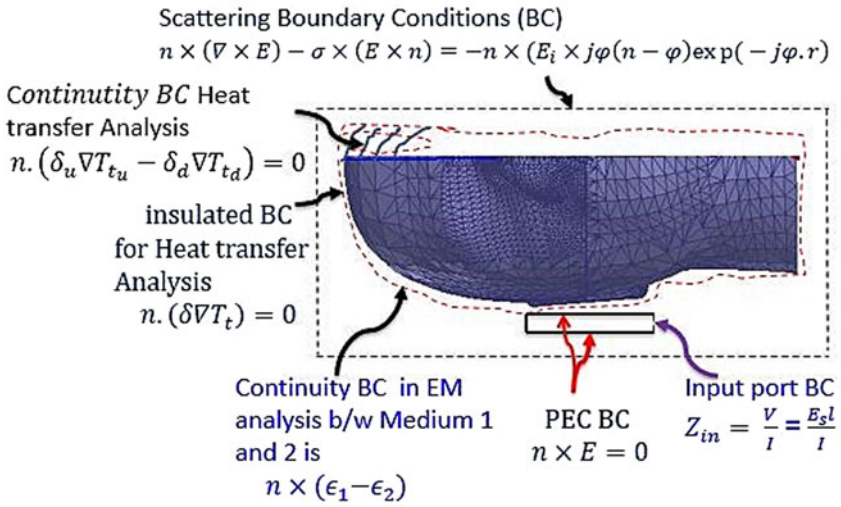

Fig. 10. Analytically explained the 3D half-human head model.

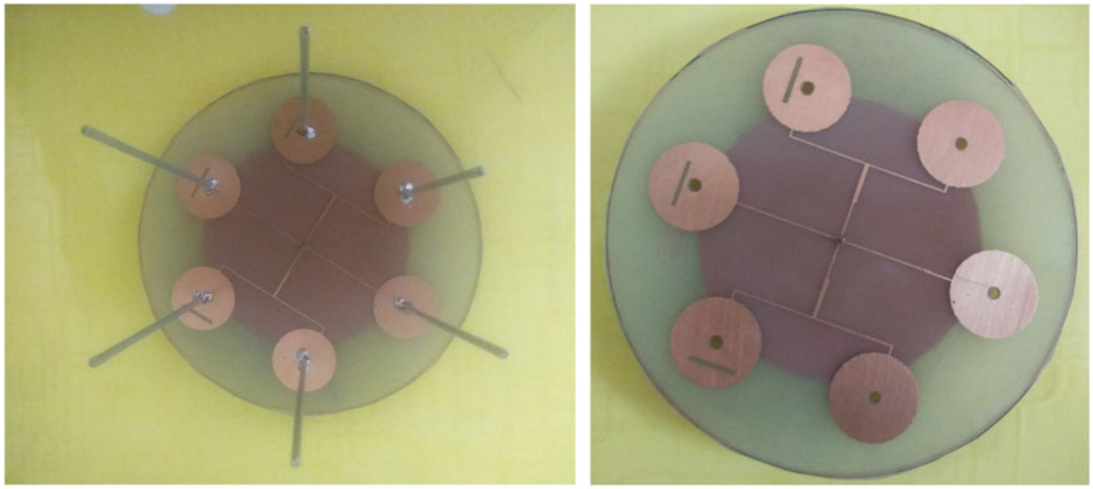

Fig. 11. Fabricated proposed array (a) without probes, (b) with probes.

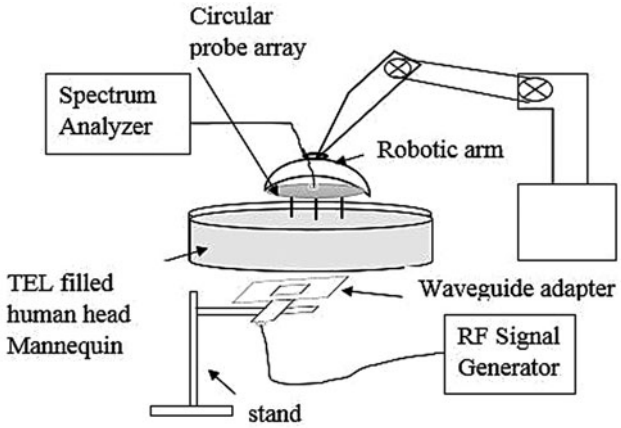

Fig. 12. SAR measurement prototype.

Table 2. Ingredients weights in percentage

Freq. in (GHz)	DGBE (%)	Triton x-100 (%)	Nacl (%)	Water (%)
1.8	44.92	30.45	0.18	54.90
2.1	50	19.97	0.16	71.97
2.4	7.99	19.97	0.16	49.75
2.5	7.99	19.97	0.16	71.88

To verify the assumptions, the 3D human head model has been created in the free space environment with scattering boundary conditions. The interaction of electromagnetic wave propagation on the half-human head model analysis has been presented by

https://doi.org/10.1017/S1759078722000101 Published online by Cambridge University Press

Table 3. Measured results

Freq. (GHz)	ε'	ε''	E (V/m) Sim.-Mea.	ω	ε	σ (S/m)	Sim. SAR 1 g (W/kg)	Mea. SAR 1 g (W/kg)	TRP (dBm)
1.88	53.28	15.17	4.00–9.45	1.13 × E + 09	8.85E – 12	1.52	0.02372	0.13574	21–23
2.10	53.28	13.90	3.71–8.20	1.32E + 10	8.85E – 12	1.61	0.02162	0.108256	15–17
2.45	52.68	14.30	3.42–9.30	1.54E + 10	8.85E – 12	1.94	0.02213	0.167791	11–15
2.50	52.62	14.53	3.14–11.0	1.57E + 10	8.85E – 12	2.02	0.01943	0.24442	11–18

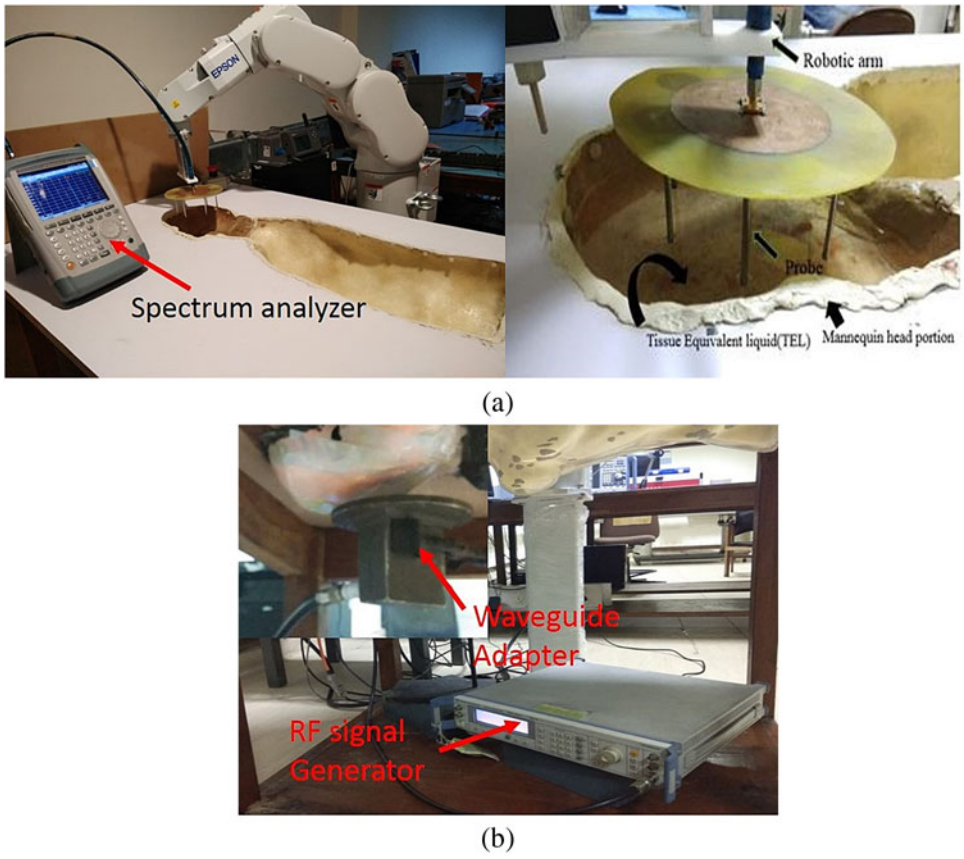

Fig. 13. (a) Top view, (b) bottom view of SAR measurement setup.

using Maxwell equations as follows [18–21].

$$\nabla \times \frac{1}{\mu_r} \nabla \times E - \varphi_o^2 \varepsilon_r E = 0, \tag{9}$$

$$Z_{in} = \frac{V}{I} = \frac{E_s l}{I}, \tag{10}$$

where Z_{in} is the input impedance in (ohms), V is the edge voltage (v), I is the electric field current, l is the edge length,E_s is the E-field of the source, $\varphi_o$is the free space wavenumber (m^{-1}).

$$n \times E = 0. \tag{11}$$

For the patch antenna, perfect electric condition (PEC) inner and outer boundary condition (BC) between the two mediums is

$$n \times (\epsilon_1 - \epsilon_2). \tag{12}$$

Truncated free space scattering boundary conditions are

$$n \times (\nabla \times E) - \sigma \times (E \times n) = -n \times (E_i \times j\varphi(n - \varphi)\exp(-j\varphi.r), \tag{13}$$

where $\sigma = j\varphi n$ is electric conductivity, E_i is an incident plane wave, $j = \sqrt{-1}$, φ is the wavenumber (m−1).

The temperature distribution within the human head has been evaluated by using the penne bio-heat analysis as per Maxwell equations [18, 19]. According to the ICNIRP guide standard

https://doi.org/10.1017/S1759078722000101 Published online by Cambridge University Press

Table 4. Standard limits

Freq. (GHz)	ε	σ (S/m)	SAR 1 g, 10 g (W/kg) [ICNIRP]
1.8	40.4	1.40	1.6, 2
2.1	41.1	1.55	
2.4	39.2	1.82	
2.5	39.2	1.82	

[1], another definition of SAR in accordance with temperature distribution is given in equation (16).

$$\rho C\frac{\partial T}{\partial t} = \nabla.(k\nabla T) + \rho_b C_b \omega_b (T_b - T) + Q_{met} + Q_{ext}, \quad (14)$$

$$Q_{ext} = \frac{1}{2}\ \sigma_{tissue} E^2 = \frac{\rho}{2}\ .SAR, \quad (15)$$

$$SAR = C\frac{\partial T}{\partial t} = \frac{\sigma}{\rho}\ E^2, \quad (16)$$

where ρ is the tissue density (kg/m^3), C is the heat capacity of the tissue (J/kg K), δ is the thermal conductivity of tissue (W/m K), T is the tissue temperature (°C), T_b is the temperature of blood (°C), ρ_b is the density of blood (kg/m^3), $C_b$is the heat capacity of blood (3960 J/kg K), ω_b is the blood perfusion rate (1/s), Q_{met} is the metabolism heat source (W/m^3), and Q_{ext} is the external heat source (electromagnetic heat-source density) (W/m^3).

The external heat source term is equal to the resistive heat generated by the electromagnetic field [electromagnetic power absorbed (P_a)], which is defined as [18].

$$P_a = Q_{ext}\ = \frac{\sigma_{tiss}}{2}\ E^2 = \frac{\rho}{2}.SAR. \quad (17)$$

The heat transfer is considered only in the human head, which does not include parts of the surrounding space. As shown in Fig. 10, the outer surface of the human head corresponding to assumption (11) is considered to be a thermally insulated boundary condition as given below in equation.

$$n.(\delta\nabla T_t) = 0. \quad (18)$$

It is assumed that no contact resistance occurs between the internal organs of the human head. Therefore, the internal boundaries are assumed to be continuous as follows

$$n.(\delta_u \nabla T_{t_u} - \delta_d \nabla T_{t_d}) = 0. \quad (19)$$

Figure 10 portrays an analytical analysis of the electromagnetic spectrum penetration on the human head when we use mobile phones, as well as how electromagnetic radiation pretends to incrementally heat with respect to time. Table 3 showcases the experimental results based on equations (1–4).

Measurement discussion

To evaluate the design approach, the proposed design was fabricated and measured as shown in Figs 11 and 12. The return loss of simulated and measured results within the good agreement has been observed as shown in Fig. 4. Because of manufacturing and binding of SMA connector using a conductive adhesive, there was little resonance variation in measured results compared to simulated. The proposed circular microstrip patch antenna is designed in Ansys High-Frequency Structure Simulator (HFSS). To investigate the

Table 5. Uncertainty estimation

Source of uncertainty				Standard uncertainty (Us_t) V/m				
Type	Contribution	Uncertainty value V/m	Probability distribution/Div	1.8 GHz	2.1 GHz	2.4 GHz	2.5 GHz	D_f
A	Repeatability	0.23, 0.46 0.85, 1.62	$N\ \sqrt{8}$	0.081	0.162	0.300	0.572	7
B	Electric field	0.009	$U\ \sqrt{3}$	0.005	0.005	0.005	0.005	∞
	Nonlinearity	0.020	N 2.6	0.007	0.007	0.007	0.007	∞
	Frequency	0.042	N 2.6	0.016	0.016	0.016	0.016	∞
	Conductivity	0.126	$R\ \sqrt{3}$	0.072	0.072	0.072	0.072	∞
	Permittivity	0.202	$R\ \sqrt{3}$	0.116	0.116	0.116	0.116	∞
	Temperature	0.260	$R\ \sqrt{3}$	0.150	0.150	0.150	0.150	∞
	Combined uncertainty		$U_c = \sqrt{\sum_{i=1}^{7} U_{st}^2}$	0.219	0.260	0.362	0.607	
	Coverage factor		$k = 2$					
	Expanded uncertainty		$U_e = KxU_c$	0.438	0.520	0.725	1.214	

Where N, normal; *U*, uniform; *R*, rectangular; D_f, degree of freedom.

https://doi.org/10.1017/S1759078722000101 Published online by Cambridge University Press

Table 6. Comparison of proposed and earlier publications

Ref.	Freq. in (GHz)	Input power	Phantom type	Type	SAR (W/kg) 1–10 g
[28]	2.45	100 mW	SAM	CPW microstrip	0.54
[29]	2.48	2 mW	Head model	Microstrip	0.36
[30]	0.92	1 mW	Head model	Microstrip	0.33
[31]	0.46	1 mW	Head model	Microstrip	0.69
Proposed	1.8–2.50	1 W	Head Mannequin	Circular microstrip	0.13–0.24

SAR values of fabricated design, the human tissue-equivalent liquid (TEL) is essential. Hence, as per IEEE 1528 standard, for the TEL preparation, four ingredients are integrated, i.e. DGBE, Triton x-100, NaCl, and distilled water. These ingredient weights of percentage vary with respective frequencies as shown in Table 2.

Figure 12 is a quasi-human body mannequin model used to investigate SAR experimentally [22–24]. The top and bottom view of the human head mannequin model is shown in Figs 13(a) and 13(b). In this measurement, RF signal generator is the input source fed by 1 Watt power at the selected frequency from 1.8 to 2.5 GHz. The RF source connected with the waveguide adapter aligned below the center of the mannequin to feed the exposer, which is near to the ear as shown in Fig. 10 representing PEC BC. The designed circular probe array is connected with a spectrum analyzer and integrated with a robotic arm at the center of the TEL-filled human head mannequin to measure the instantaneous E-field values at six different positions as shown in Fig. 13. The simulated and measured electric field/SAR values, as well as total radiated power (TRP) values, are presented in Table 3.

The measured SAR values are given in Table 3. In this measurement complex, permittivity and conductivity values are measured by using DAK 3.5 dielectric probe [15]. For the SAR evaluation, electric field plays a major role, i.e. E-field is directly proportional to the SAR from equation (1). The obtained E-filed values are measured by using the proposed design, and after comparison of Tables 3 and 4, the obtained SAR values are within the standard limits. As per IEC-62209-1,2,3/IEEE 1528 [25–27], the circular probe array each source of uncertainty budget evaluation has been performed as shown in Table 5. Soh *et al.* have reported a SAR value of 0.54 W/kg in reference [28], but the proposed work obtained a SAR value of 0.24 W/kg; the difference may vary due to the repeatability of the test. The comparison of earlier to present existing work of SAR evaluation has been presented in Table 6.

Conclusion

This study demonstrates a new approach of circular disk microstrip patch probe antenna array for simultaneous precise SAR measurement at quad-band frequencies. In the design aspect, various parameters of the antenna are optimized and optimum design is presented. The proposed antenna return loss is $S_{11} < -10$ dB, and SAR was evaluated for 1 g of biological tissue; the obtained results are within the ICNIRP and ANSI/IEEE safety standard limits. The circular antenna array each source of uncertainty budget has been estimated precisely, therefore, this probe may advisable for SAR evaluation.

Acknowledgement. The author would like to thank Dr. S. K. Dubey for lab facility and Dr. Rina Sharma, Director of NPL for their constant motivation and support throughout this work, and CSIR-HRDG.

Conflict of interest. None.

References

1. **International Commission on Non-Ionizing Radiation Protection (ICNIRP)** (2020) Guidelines for limiting exposure to electromagnetic fields (100 kHz to 300 GHz). *Health Physics* **118**, 483–524.
2. **Anderson V** (2003) Comparison of peak SAR levels in concentric sphere head models of children and adults for irradiation by a dipole at 900 MHz. *Physics in Medicine and Biologyl* **48**, 3263–3275.
3. **Martinez-Burdalo M, Martin AA, Anguiano M and Villar R** (2004) Comparison of FDTD-calculated specific absorption rate in adults and children when using a mobile phone at 900 and 1800 MHz. *Physics in Medicine and Biology* **49**, 345–354.
4. **Gandhi OP and Kang G** (2002) Some present problems and a proposed experimental phantom for SAR compliance testing of cellular telephones at 835 and 1900 MHz. In Parodi K and Baffa O (eds), *Physics in Medicine and Biology*, vol. **47**. London, UK: Inst. Phys, pp. 1501–1518.
5. **Mochizuki S, Watanabe S, Taki M, Yamanaka Y and Shirai H** (2004) Size of head phantoms for standard measurements of SAR due to wireless communication devices. *Electronics and Communications in Japan (Part I)* **87**, 82–91.
6. **Wang J and Fujiwara O** (2003) Comparison and evaluated of electromagnetic absorption characteristics in realistic children for 900-MHz mobile telephones. *IEEE Transactions on Microwave Theory and Techniques* **51**, 966–971.
7. **Gandhi OP, Lazzi G and Furse CM** (1996) Electromagnetic absorption in the human head and neck for mobile telephones at 850 and 1900 MHz. *IEEE Transactions on Microwave Theory and Techniques* **44**, 1884–1897.
8. **Schoenborn F, Burhardt M and Kuster N** (1998) Difference in energy absorption between heads of adults and children in the near field of sources. *Health Physics* **74**, 160–168.
9. **Hadjem A, Lautru D, Dale C, Wong MF, Fouad-Hanna V and Wiart J** (2004) Comparison of specific absorption rate (SAR) induced in child-sized and adult heads using a dual-band mobile phone. In IEEE MTT-S International Microwave Symposium Digest.
10. **IEEE C95.1-2005** (2005) IEEE standards for safety levels with respect to human exposure to radio frequency electromagnetic fields, 3 kHz to 300 GHz. Institute of Electrical and Electronics Engineers, Inc. New York, NY.
11. **IEEE Standard for Safety with Respect to Human Exposure to Radiofrequency Electromagnetic Fields** (1999) 3 kHz to 300 GHz, IEEE standard C95.
12. **Bernardi P and Pisa S** (1998) Specific absorption rate and temperature increases in the head of cellular-phone user. *IEEE Transactions on Microwave Theory and Techniques* **48**, 1118–1126.
13. **Swadi HL and Abduljabar AA** (2020) Modelling of mobile electromagnetics wave effects on the human head. *IOP Conference Series: Materials Science and Engineering*. IOP Publishing.
14. **Jamal R, Singh RK and Singh E** (2020) Interaction of electromagnetic fields (100 kHz–300 GHz) exposure with respect to human body model and methods for SAR measurement. In Harvey D, Kar H, Verma S and Bhadauria V (eds), *Advances in VLSI, Communication, and Signal Processing*. Singapore: Springer, pp. 279–294.
15. https://speag.swiss/products/dak/dak-dielectric-probe-systems/dak-3-5-200-mhz-20-ghz/.

https://doi.org/10.1017/S1759078722000101 Published online by Cambridge University Press

16. **Balanis CA** (2007) *Antenna Theory, Analysis and Design*, 3rd Edn. New York: John Wiley & Sons, Inc.
17. **Garg R, Bhartia P, Bahl I and Ittipiboon A** (2001) *Microstrip Antenna Design Handbook*. Boston: Artech House.
18. **Wessapan T, Srisawatdhisukul S and Rattanadecho P** (2012) Specific absorption rate and temperature distributions in human head subjected to mobile phone radiation at different frequencies. *International Journal of Heat and Mass Transfer* **55**, 347–359.
19. **Wessapan T, Srisawatdhisukul S and Rattanadecho P** (2011) Numerical analysis of specific absorption rate and heat transfer in the human body exposed to leakage electromagnetic field at 915 MHz and 2450 MHz. *ASME Journal Heat Transfer* **133**, 051101.
20. **Spiegel RJ** (1984) A review of numerical models for predicting the energy deposition and resultant thermal response of humans exposed to electromagnetic fields. *IEEE Transactions on Microwave Theory and Techniques* **32**, 730–746.
21. **Shen W and Zhang J** (2005) Modeling and numerical simulation of bio-heat transfer and biomechanics in soft tissue. *Mathematical and Computer Modelling* **41**, 1251–1265.
22. **Telecommunications Technology Council** (1990) Report of Inquiry No.38.
23. **Telecommunications Technology Council** (1997) Report of Inquiry, No.89.
24. **Bownds DJ, Gregory AP, Revillod G, Cox MG and Allal D** (2020) Calibration of reference antennas for vector measurements of SAR, NPL, UK.
25. **IEC/IEEE Measurement procedure for the assessment of specific absorption rate of human exposure to radiofrequency fields from hand-held and body-worn wireless communication devices – Part 1528** (2020) Human models, instrumentation and procedures (frequency range of 4 MHz to 10 GHz)-2020.
26. **NIST Reference on Expressing Measurement Uncertainty**. Available at http://physics.nist.gov/cuu/Uncertainty/index.html.
27. **Gregory AP, Quéléver K, Allal D and Jawad O** (2020) Validation of a broadband tissue-equivalent liquid for SAR measurement and monitoring of its dielectric properties for use in a sealed phantom. *Sensors* **20**, 2956.
28. **Soh PJ, Vandenbosch G, Wee FH, van den Bosch A, Martinez-Vazquez M and Schreurs D** (2015) Specific absorption rate (SAR) evaluation of textile antennas. *IEEE Antennas and Propagation Magazine* **57**, 229–240.
29. **Chowdhury T, Farhin R, Hassan RR, Bhuiyan MS and Raihan R** (2017) Design of a patch antenna operating at ISM band for brain tumor detection. In 2017 4th International Conference on Advances in Electrical Engineering (ICAEE) IEEE.
30. **Nesar MS, Chakma N, Muktadir MA and Biswas A** (2018) Design of a miniaturized slotted T-shaped microstrip patch antenna to detect and localize brain tumor. In 2018 International Conference on Innovations in Science, Engineering and Technology (ICISET) IEEE.
31. **Uddin MN, Hasan RR, Rahman MA, Nath SK and Sarkar P** (2019) Bio-implantable antenna at human head model. In 2019 International Conference on Robotics, Electrical and Signal Processing Techniques (ICREST) IEEE.

Bhukya Venkanna Naik received his B.Tech. degree (Electronics and Communication Engineering) from the Jawaharlal Nehru Technological University, Hyderabad. He worked as a Hardware Design Engineer in the Electronics Corporation of India Limited Hyderabad. Currently, he is IEEE MTT-S, Antenna and Propagation Society member since 2017, and working toward a Ph.D. degree in RF and Microwave Engineering at the Academy of Scientific and Innovative Research (AcSIR), CSIR-NPL, New Delhi, India.

https://doi.org/10.1017/S1759078722000101 Published online by Cambridge University Press